IAC-20-B1.5.12

A System-level Engineering Approach to define the Social Value Rating of Earth Remote Sensing Missions through Sustainable Development Goals

Marcello A. Scalera[a], Marco Nugnes[b]*, Colombo Camilla[c]*

[a] *Department of Aerospace Science and Technology, Politecnico di Milano, Via La Masa 34, Milano, 20156, Italy*, marcelloagostino.scalera@gmail.com
[b] *Department of Aerospace Science and Technology, Politecnico di Milano, Via La Masa 34, Milano, 20156, Italy*, marco.nugnes@polimi.it
[c] *Department of Aerospace Science and Technology, Politecnico di Milano, Via La Masa 34, Milano, 20156, Italy*, camilla.colombo@polimi.it
* Corresponding Author

Abstract

In 2015, the UN state members agreed on the "Transforming our world: the 2030 Agenda for Sustainable Development" document to drive the evolution of humanity in the close future. A great effort has been placed to understand how space missions and their data can support the goals fulfilment, both by private entities and public organisations like the European Space Agency (ESA) or United Nations Office for Outer Space Affairs (UNOOSA).

This paper proposes a method to evaluate the level of support that a space missions used for Earth observation in Low Earth Orbit (LEO) can provide to each goal, using a set of indices based on missions' and payloads' performance related to Earth Observation (EO) services. Eight Earth observation services have been selected for this study: mapping, disaster monitoring, forestry, agriculture, geology, oceanography, hydrology, meteorology.

Each of these services has its own performance requirements and can support many different goals. Using the relationship between mission performance and services together with the original correlation between the services and the Sustainable Development Goals 2030 (SDG2030), the final assessment of an Earth Observation mission towards each goal is achieved.
Keywords: Earth observation, sustainable development goals 2030, LEO, United Nations.

Nomenclature

FSI	final service index
I_{sr}	space resolution index
I_{tr}	time resolution index
I_{spctr}	spectral efficiency index
n	number of orbits in repeat cycle
QI	Quality Indices
SEf	Social Efficiency index
SI	Services Indices
T_{orbit}	orbital period [s]

Acronyms/Abbreviations

EO	Earth Observation
ESA	European Space Agency
GSD	Ground Sample Distance
HRVIR	Haute Résolution dans le Visible et l'Infra-Rouge
IFOR	Instantaneous Field Of Regard
IFOV	Instantaneous Field Of View
LEO	Low Earth Orbit
NIR	Near Infrared
SEF	SDG Efficiency Index
SI	Services Indices
SDG	Sustainable Development Goals
SAR	Synthetic Aperture Radar
TIR	Thermal Infrared
UCS	Union of Concerned Scientists
UN	United Nations
VIS	Visible

1. Introduction

According to the most recent estimates provided by various sources like ESA, UNOOSA, Union of Concerned Scientists (UCS), the LEO region is by far the most exploited region in space and around half of the spacecraft here is devoted to Earth Observation.

The data generated by these space missions are used for a large variety of purposes and services, like those listed in Sandau et al. [4], and consequently to support the SDGs. Many documents and papers about this topic can be found in literature. In particular, the official documents by UNOOSA [6],[7] give the most detailed analysis available in literature. They focus on specific missions and on the use of their data to support some SDGs in some relevant test cases, but do not provide a general approach to the support evaluation problem. They use as starting point the data generated by the mission rather than the performance of the payloads.

Additional papers like Anderson et al. [8] give a qualitative analysis on the topic of EO data supporting the SDGs without using a quantitative approach based on mission specifics. Sarelli et al. [9] focus on the use of EO data to support specific areas of peculiar SDGs, like the SDG 14.

This paper defines a different approach where all the previously listed works are used at middle step to quantitatively assess the support of a generic space mission to the SDGs, basing on mission and payload specifics and performance.

The first step is to define payload performance and to compare it with the requirements of eight general services according to the paper by Sandau et al. [4]. These services are agriculture, disaster monitoring, forestry, geology, hydrology, mapping, meteorology, and oceanography. This is done using four Services Indices (SI), so called because they assess the effectiveness of a payload towards the previously mentioned services basing on four parameters that are space resolution, time resolution, spectral efficiency, and Earth coverage efficiency.

The next step is to link the eight EO services to the SDG2030 using the available documentation on the topic previously cited as baseline for this process. It is then possible to compute quantitatively the support of the analysed payloads to 17 SDGs.

Another set of four indices called Quality Indices (QI) has been developed to assess the quality of the operating environment of the mission, focusing on the negative effects generated by orbital overcrowding (based on UCS [3] data) and debris (based on Maury et al. [10]), on Earth accessibility using ESA ground station network (described by ESTRACK [11]) and on needed orbit maintenance effort (Curtis [12], Griffin [13], Wertz and Larson [14], Fortescue et al. [15], Battin [16] and Sissenwine et al. [17]).

The paper is structured as follows. In Section 2 the four SI are described in deep details. They are then used in Section 3 to define the computation of the support to the SDGs. Section 4 gives a comprehensive description of the four QI. Finally, Section 5 concludes the paper presenting the conclusions and the possible future developments.

2. Services indices

Services indices are based on the comparison between the performance of an analysed payload and those required by the selected eight services, focusing on four different parameters: space resolution, time resolution, spectral efficiency, Earth coverage efficiency. All indices have been scaled such that their range lies between 0 (lowest figure of merit) to 100 (highest figure of merit).

2.1 Space resolution index

The first SI focuses on the evaluation of payload performance in terms of spacial resolution defined as its Ground Sampling Distance (GSD). This has been done starting from the payload and mission data rather than using already delivered data. This way the method can be used also in the design phase of payload and missions that are still to be defined. The computations have been carried out for single and multiple Whiskbroom sensors, Pushbroom sensors and matrix imagers in the visible (VIS), near infrared (NIR), thermal infrared (TIR) spectral ranges. The resolution of these passive sensors has been computed following Wertz and Larson [16], Fortescue et al. [17], Kramer [18]. Synthetic Aperture Radar (SAR) antennas have been studied and modelled as well following Moreira et al. [19], Moreira [20] and Kuenzer [21].

Once the space resolution (from now on also called as GSD) of the considered payload is computed, it is possible to compare it with respect to the requirements of each service. These values have been obtained by Sandau et al. [4] and they are shown in Fig. 1 together with the revisit time requirements for all considered services.

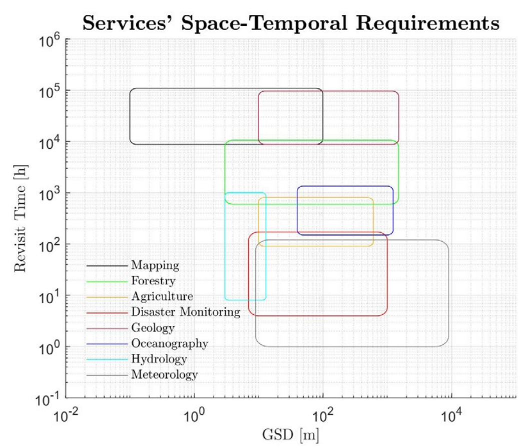

Fig. 1. Space and time resolution performance required by selected services. Courtesy of Sandau [4]

The boundary levels for each service regarding space resolution are summarised in Table 1.

The computation of the space resolution index can now be defined. It is based on the distance between the operative point, identified by the studied payload's GSD performance, and the boundaries of the required performance region for each service. This evaluation evolves in the space resolution index formula shown in Eq. (1) and graphically in Fig. 2.

$$I_{sr} = \frac{GSD_{serv,max} - GSD_{payload}}{GSD_{serv,max} - GSD_{serv,min}} \% \qquad (1)$$

Table 1. Space resolution performance boundaries of the services

Service	$GSD_{serv,min}$ [m]	$GSD_{serv,max}$ [m]
Agriculture	10	600
Disaster Monitoring	7	1000
Forestry	3	1400
Geology	10	1500
Hydrology	2	15
Mapping	0.1	100
Meteorology	9	9000
Oceanography	40	1200

According to this definition, the index can range between -∞ and +∞. However, it is needed that this index lies in the interval [0,100] to be comparable with the following one. It is then decided to make any value above 100, meaning that payload GSD is better than the minimum boundary, equal to 100 and any negative value, meaning that payload GSD is worse than the maximum boundary, equal to 0.

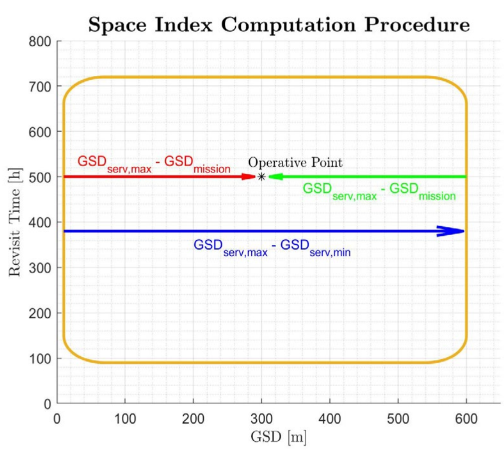

Fig. 2. Representation of space resolution index computation

As test cases, the passive payloads onboard of SPOT-4 have been selected. Even if it represents an old mission, they have been selected due to the high amount of reliable information available due to their long operative time. They are named HRVIR and Vegetation. HRVIR is a high resolution, low IFOV passive sensor with the ability of off-nadir pointing. Vegetation is a large IFOV, low resolution passive sensor that cannot perform off-nadir observations. It should be clear that these sensors have been developed following two opposite design philosophies, making their comparison even more interesting for all the SI and their FSI.

In Table 2, the GSDs of HRVIR in both nadir and off-nadir pointing, and of Vegetation are presented. The results have been validated comparing them with the literature available about these sensors.

Table 2. GSD of HRVIR and Vegetation.

Sensor	$GSD_{payload}$ [m]
HRVIR (Nadir pointing)	19.8
HRVIR (Off Nadir pointing)	27.45
Vegetation	1120

Now it is possible to compute the space resolution index for HRVIR and Vegetation sensors for each of the considered services. The results are shown in Fig. 3.

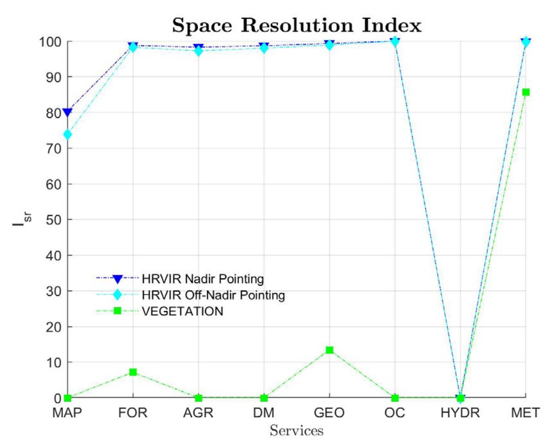

Fig. 3. Space resolution index results for HRVIR and Vegetation

Regarding active SAR sensors, the index computation is the same. The only and crucial difference regards how to compute the antenna's GSD. However also the SAR GSD computation has been verified comparing with results found in literature.

2.2 Time resolution index

The time resolution index computation is similar to the space resolution one. However, it can be considered as the complementary of the space resolution index because a fast revisit time is related to a large Instantaneous Field of Regard (IFOR) or IFOV that translates in a poor space resolution. This index is based on the comparison between the studied payload's performance and the services requirements, just like the previous one. Once again, the services requirements are recovered by Sandau et al. [4] as already shown in Section 2.1 in Fig. 1. They are summarised in Table 3.

Table 3. Revisit time boundaries of the services.

Service	$T_{serv,min}$ [h]	$T_{serv,max}$ [h]
Agriculture	90	720
Disaster Monitoring	4	168
Forestry	600	10^4
Geology	8766= 1 *year*	87660= 10 *year*
Hydrology	8	10^3
Mapping	8766= 1 *year*	10^5
Meteorology	3	120
Oceanography	150	1200

Focusing on LEO missions, the revisit time concept makes sense only if the payload and its spacecraft are placed on a repeated groundtrack orbit. The revisit time of an orbit, defined as the time interval between two consecutive passages over the same Earth surface location, has been computed according to Wertz and Larson [14], Fortescue et al. [15] and Boain [20]. It is possible to compute the distance between successive groundtracks placed by consecutive orbits. This distance ΔL is progressively filled by the orbits of the other days of the repeat cycle. At the last day of the repeat cycle, all groundtracks have been set, and the distance among them is reduced to the minimum as possible; this is the distance among adjacent groundtracks δl. This process is shown for a m/n = 8/117 orbit in Fig. 4, where m is the number of days of the repeat cycle and n is the number of orbits completed during the repeat cycle.

It is easy to see that each day the maximum distance between cumulated groundtracks reduces. When the GFOR of the payload gets larger than the maximum distance among the cumulated groundtracks of a specific day, it means that the sensor is revisiting some locations on Earth surface. This specific day defines the revisit time of the sensor.

The procedure is shown in Fig. 5, where D_i is the vector that contains the k distances among cumulated groundtracks at day i, $T_{mission}$ or RVT is the payload revisit time and T_{orbit} is the orbital period. It may also happen that the maximum distance among cumulated groundtracks is larger than the IFOR for all the repeated cycle. In this case the revisit time is simply equal to m and the global coverage cannot be achievable.

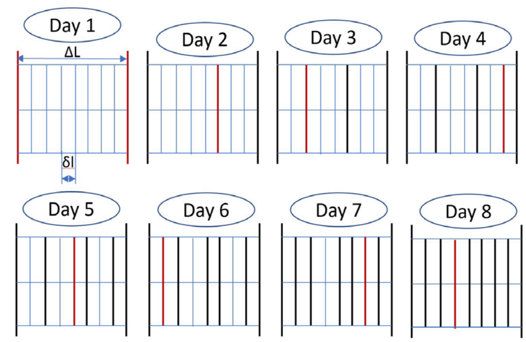

Fig. 4 Groundtrack evolution of an m/n=8/117 orbit during all days of the repeat cycle. In red there are the groundtrack placed in reported day and in black the groundtracks placed in previous days

In the simple case of a constellation made of satellites on the same orbital plane and equally spaced, the constellation revisit time is the single satellite's one divided by the number of satellites in the constellation, according to Fortescue et al. [15]. This is a very common EO constellation parameter and the only one considered in this paper.

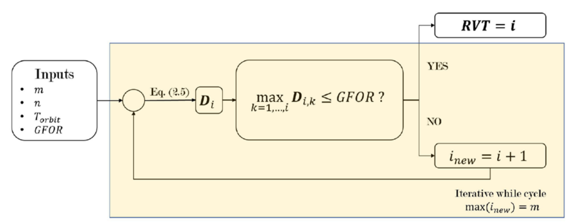

Fig. 5 Revisit time computation method

Once the revisit time of the payload is obtained, it is possible to compute the time resolution index as shown in Eq. (2) and graphically in Fig. 6.

$$I_{tr} = \frac{T_{serv,max} - T_{mission}}{T_{serv.max} - T_{serv.min}} \% \quad (2)$$

As for the space resolution index, the results are artificially limited to the range [0,100]. Indices above 100 resulting from a faster revisit time than the minimum boundary are limited to 100. Negative values representing revisit times longer than the maximum boundary are made equal to 0.

Also in this case, the payloads onboard of SPOT-4 have been used as test cases. In Table 4, the results of the time resolution for these payloads are summarised.

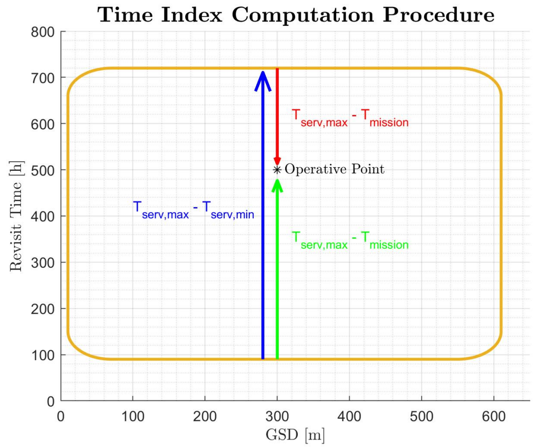

Fig. 6 Representation of time resolution index computation

Table 4. GSD of HRVIR and Vegetation.

Sensor	$T_{mission}$ [days]
HRVIR (Nadir pointing)	26
HRVIR (Off Nadir pointing)	5
Vegetation	3

These data can be used to compute the time resolution index for HRVIR and Vegetation. The results are shown in Fig. 7.

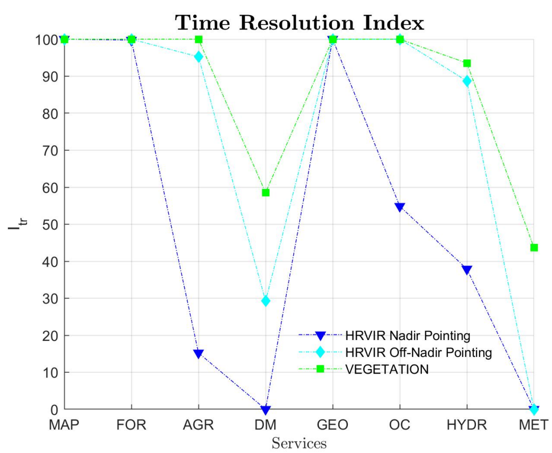

Fig. 7. Time resolution index for HRVIR and Vegetation

For some services, the time resolution index is 100 for every payload. This is due to the very weak performance requirements related to some services like mapping. For other services it is clear how a trade-off between high values of this index and high values of space resolution index must be done.

2.3 Spectral efficiency index

This index evaluates how well the payload can detect specific parameters for each service. The distinction among the regions of the electromagnetic spectrum at which the sensors work becomes crucial. The spectral regions considered are VIS-NIR and TIR (divided in two parts related to atmospheric transparency according to Kuenzer [21]) for passive sensors and microwaves, and for SAR active antennas, respectively.

2.3.1 Passive sensors in VIS-NIR spectral region

In the case of passive sensors in VIS-NIR spectral region, the index is based on the reflectivity of the Earth surface in the VIS-NIR region. This is meaningful because these sensors operate by detecting the electromagnetic radiation reflected by the Earth surface. The reflectivity values of Earth have been collected by USGS database [22][23][24]. These coefficients have been linked to the services that rely on their detection like forestry as shown in Fig. 8. The values of reflectivity of trees and grass reported are coming from an average on various species of trees and grasses available on the USGS database.

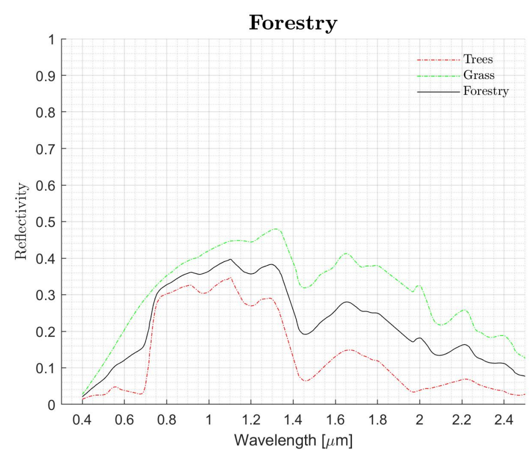

Fig. 8. Forest reflectivity

Once this procedure is repeated for all the services, the sensors operative wavelengths in the VIS-NIR region are used to compute the index. The sensors HRVIR and Vegetation are still used as reference since they both operate only in the VIS-NIR region exploiting the same bands summarised in Table 5.

It is now possible to compute the spectral efficiency index for the VIS-NIR operating sensors. The operative bands for HRVIR and Vegetation can be represented together with the reflectivity plots of all services, as shown in Fig. 9.

Table 5. Operative spectral bands of HRVIR and Vegetation.

Band	Spectral range [µm]	Region
1	0.50 – 0.59	VIS
2	0.61 – 0.68	VIS
3	0.79 – 0.89	NIR
4	1.58 – 1.75	NIR

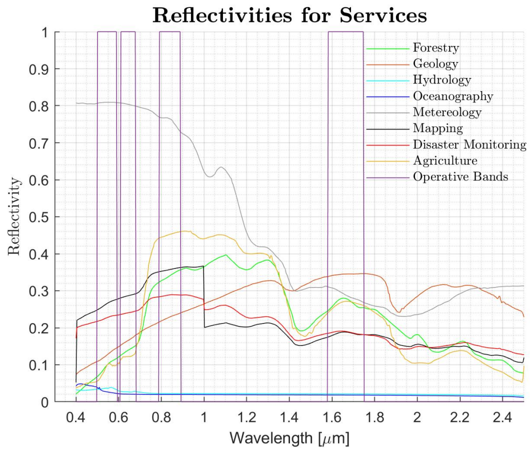

Fig. 9. Reflectivity plots for all the services and spectral operative bands of HRVIR and Vegetation

The computation of the spectral efficiency index can be finally performed. It is based on the comparison between the area below the reflectivity plots in the operative spectral regions $A_{spctr,op}$ and the total area below the reflectivity plots for each service $A_{spctr,tot}$. This is represented by Eq. (3) and graphically by Fig. 10.

$$I_{spctr} = \frac{A_{spctr,op}}{A_{spctr,tot}} \% \qquad (3)$$

Focusing on HRVIR and Vegetation, two types of results can be obtained. The first one is about the overall index value for each service considering the contribution of all spectral bands as shown in Fig. 11.

Another interesting result is represented in Fig. 12 where the index value for each operative band of the sensor is reported. It highlights the dependence on the bandwidth. Indeed, larger bands result in a higher index value on average. It is also interesting to detect which bands are more effective towards a certain service and which can be modified to focus on different features to be detected.

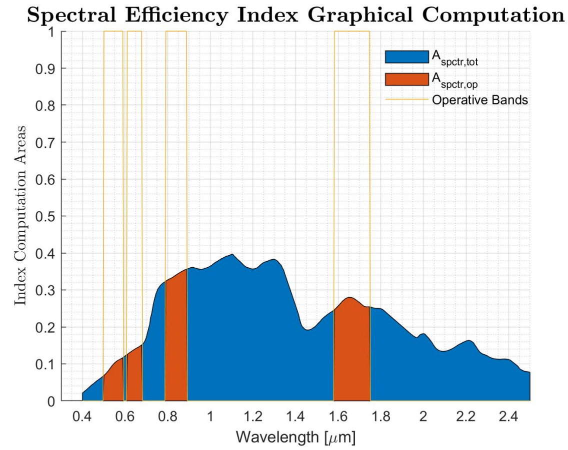

Fig. 10. Spectral efficiency index computation

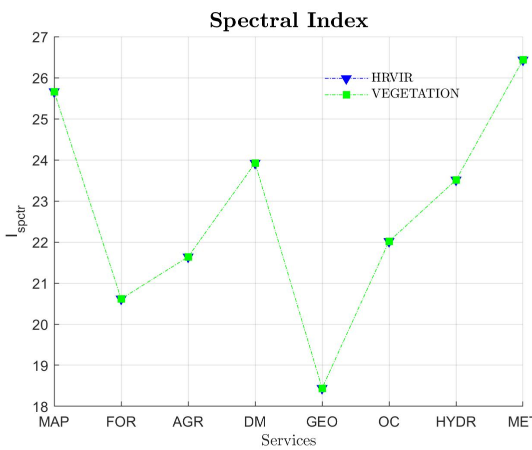

Fig. 11. Spectral efficiency index for HRVIR and Vegetation

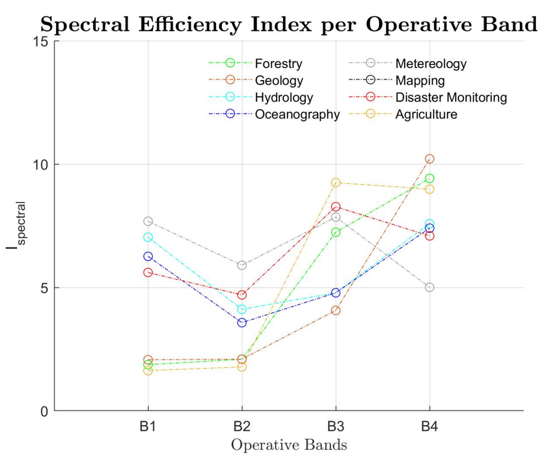

Fig. 12. Spectral efficiency index results for each operative band of HVIR and Vegetation

2.3.2 Passive sensors in TIR region

In the TIR spectral region, the spectral efficiency index is computed in a very similar way to the VIS-NIR region. However, there are mainly two differences. First, in this case the emissivity of Earth's surface will be used rather than the reflectivity. Secondly, according to Kuenzer [21], the TIR region is divided in two separate sub regions due to the atmospheric transparency. The first sub region stretches from 3 to 5 μm, the second from 7 to 14.5 μm. The emissivity related to all the services is shown in Fig. 13, focusing on the 3-5 μm region, and in Fig. 14, regarding the 7-14.5 μm. These are obtained from the database associated with Meerdink et al. [25].

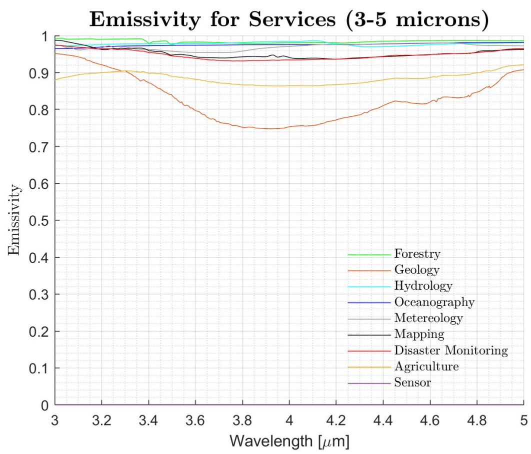

Fig. 13 Emissivity curves of the services in the 3-5 μm thermal spectral region

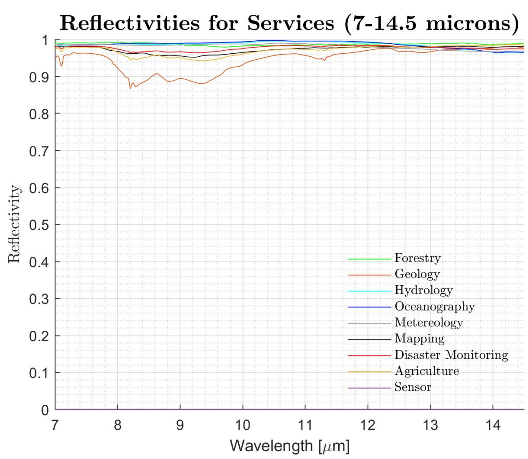

Fig. 14. Emissivity curves of the services in the 7-14.5 μm thermal spectral region

Following the comparison between the area as for the spectral efficiency region in Sec. 2.3.1 (Eq. (3) and Fig. 10), it is possible to compute a spectral efficiency index for each of the considered thermal spectral regions, namely $I_{TIR,1}$ for the 3-5 μm region and $I_{TIR,2}$ for the 7-14.5 μm region. The passage to a single index is performed using a weighted average using the weights $w_{TIR,1}$ and $w_{TIR,2}$. This is thought to address those missions that focus mainly on one of the two regions and use the other one just marginally for support activities. Using this approach, the resulting index would not be penalised. The computation of the index is then shown in Eq. (4).

$$I_{spctr} = \frac{I_{TIR,1} w_{TIR,1} + I_{TIR,2} w_{TIR,2}}{w_{TIR,1} + w_{TIR,2}} \tag{4}$$

The test case is provided by the MODIS payload onboard of the Terra and Aqua satellites, focusing only on its thermal wavelengths. The specifics about this payload and its operative spectral bands can be found in Kramer [18] and ESA [26]. Also in this case it is possible to isolate the contribution of the single bands to the overall index value.

2.3.3 Active SAR antennas

The spectral efficiency index modelling in this case is performed in a very different way with respect to the previous cases. The parameter used to build the index is the penetration depth of the waves generated by the SAR antenna in the usual materials related to each service. The penetration depth has been modelled using the theory by Nowak [27] basing on materials' real and complex parts of dielectric permittivity constants. No database regarding the dielectric permittivity constants has been found, so the needed data have been gathered by a series of papers: Shrestha et al. [28], Ulaby et al. [29], Hallikanen et al. [30], Chang et al. [31]. The resulting penetration depth is shown in Fig. 15 for forestry.

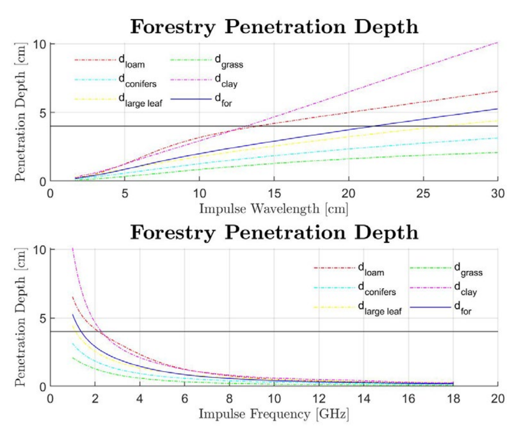

Fig. 15. Penetration depth trend versus wavelenght and frequency for forestry

Once the penetration depth for each service is computed as a function of the frequency, a desired benchmark depth for each service is needed to compute the index. These reference levels have been selected considering the typical uses of SAR and microwave imaging related to each service. They can be changed according to the payload design, to optimise the index computation and its aim.

The formula to compute the spectral efficiency index in the case of SAR active sensors is based on the difference between the desired penetration depth and the obtained one at operative frequency as shown in Eq. (5) and Eq. (6). The Eq. (5) is used if the operative penetration depth is higher than the desired one, otherwise Eq. (6) is used.

$$I_{spctr} = 100 - \left[\frac{d_{op}}{d_{serv}} 100 - 100 \right] \tag{5}$$

$$I_{spctr} = \frac{d_{op}}{dserv} 100 \tag{6}$$

Using SAR-C sensor (whose data can be retrieved in ESA [26]) as test case it is possible to show the behaviour of this index at the variation of operative frequency/wavelength, leading to Fig. 16.

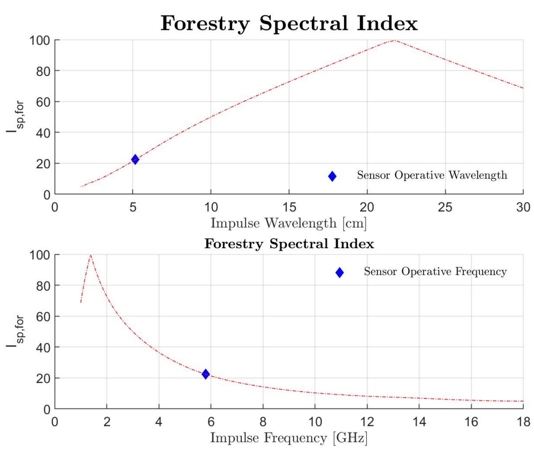

Fig. 16. Spectral index value for SAR-C sensor related to forestry

2.4 Earth coverage index

This index evaluates the efficiency of the payload in detecting specific areas on Earth's surface according to service considered. It is based on the comparison of the time passed over particular regions with the total orbital time of the repeat cycle. To perform the computations for this index the simulation of the orbit is needed along the whole repeat cycle together with the related groundtracks. Knowing the payloads' GFOR and the Sub Satellite Point (SSP), it is possible to check which areas of Earth's surface the sensor can detect and which are excluded.

A discretization of the Earth's surface has been obtained using a mesh made of all the points defined by an integer value of longitude and latitude, resulting in a 360x180 points grid on the Earth's surface. The interesting locations for each service are then selected on these maps that will be referred from now on as pixel maps. The selection of interesting areas for each service has been carried on basing on the grey scale colours of the Earth's surface. For some services, a further step of refinement of the pixel map was needed. An example is shown in Fig. 17 referring to oceanography.

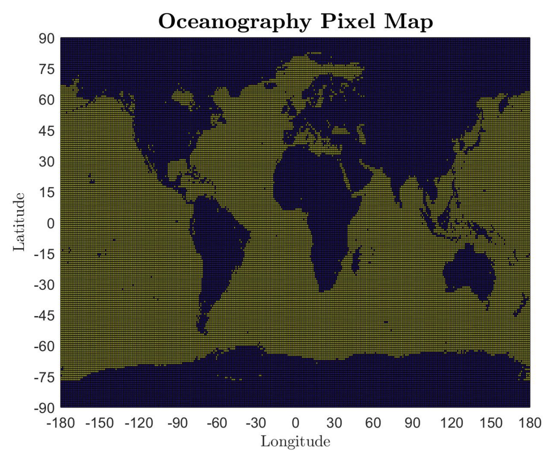

Fig. 17. Oceonography pixel map. Yellow locations are the interesting ones

A function to check the instantaneous access region at each integration step of the orbit propagation has been developed considering the SSP and the visible longitudes around it. If at least one of these points is related to a region devoted for a particular service according to its pixel map, the time step is saved as useful. This process is based on a matrix U of dimensions [n_{intgr} x n] where n_{intgr} is the number of integration steps of the orbits and n is the number of orbits in the repeat cycle. This process is graphically shown in Fig. 18.

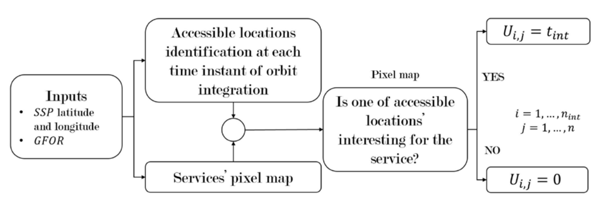

Fig. 18. Method to generate matrix U

Once the matrix U is obtained, the time instants of the orbit simulation related to the detection of the relevant regions are known. The beginning and ending time instants are stored for each of the n orbits in the repeat cycle and saved in two matrices, respectively I and E. Computing the difference E – I for each n orbit, the time passed over those regions for each of the n performed orbits (named Δ_{dtct}) is obtained as shown in Eq. (7).

$$I_{cov-orb} = \frac{\Delta T_{dtct}}{T_{orbit}} \% \tag{7}$$

The result of this computation is already meaningful since it isolates the effectiveness in terms of Earth coverage of each single orbit of the repeat cycle. The results for the already presented HRVIR sensor are shown in Fig. 19.

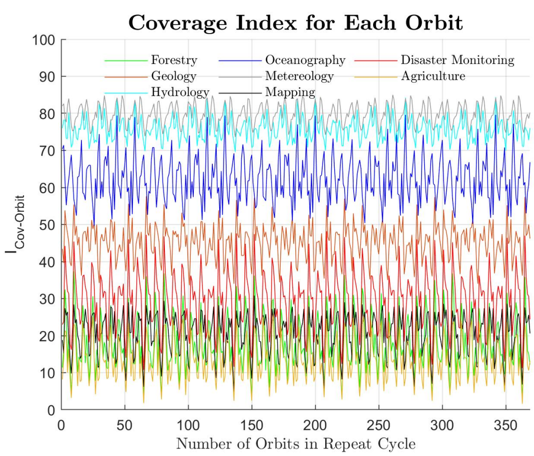

Fig. 19. HRVIR coverage index result for each orbit repeat cycle

For each service, a single value of the Earth coverage index is needed to perform the following computations. Therefore, the results related to each orbit in the repeat cycle must be condensed in a single value for the Earth coverage index of the payload. This is done performing the average of the single orbit coverage index for all the orbits, as described in Eq. (8), where *i* is the counter of orbits that goes up to *n,* that is the number of completed orbits in the repeat cycle.

$$I_{cov} = \frac{\sum I_{cov-orb,i}}{n} \tag{8}$$

3. Index of support to the Sustainable Development Goals 2030

In this section the SI presented in Section 2 will be used to compute the support that a payload can offer to the 17 SDGs. It is essential to define the relationships between the SDGs and the services. This is done basing mainly on UN's official documentation regarding the SDGs (United Nations[5], UNOOSA [6][7], Copernicus Programme [32]).

The relationships among the SDGs and the services are listed in Table 6.

Table 6. List of the SDGs and related services.

SDGs	Related Services
1 – No poverty	Mapping Disaster Monitoring Agriculture
2 – Zero hunger	Mapping Forestry Agriculture Disaster Monitoring Geology Hydrology
3 – Good health and well being	Mapping Forestry Disaster Monitoring Geology Hydrology Oceanography Meteorology
4 – Quality education	Mapping
5 – Gender equality	Mapping Oceanography
6 – Clean water and sanitation	Mapping Forestry Geology Hydrology Oceanography Meteorology
7 – Affordable and clean energy	Mapping Geology Meteorology
8 – Decent work and economic growth	Mapping Forestry Agriculture Geology Hydrology Oceanography
9 – Industry, innovation and infrastructure	Mapping Geology Hydrology
10 – Reduced inequalities	Mapping Disaster Monitoring Oceanography

11 – Sustainable cities and communities	Mapping Forestry Disaster Monitoring Geology Hydrology Oceanography Meteorology
12 – Responsible production and consumption	Forestry Geology Hydrology Oceanography Meteorology
13 – Climate action	Forestry Disaster Monitoring Geology Hydrology Oceanography Meteorology
14 – Life below water	Hydrology Oceanography
15 – Life on land	Forestry Geology Hydrology
16 – Peace, justice and strong institutions	Mapping Disaster Monitoring Oceanography
17 – Partnership for the Goals	Mapping Forestry Agriculture Disaster Monitoring Geology Hydrology Oceanography Meteorology

Once the relationships between services and SDGs have been defined, the SI can be used to compute the overall contribution to the SDGs through one last manipulation needed to condense all the four indices in a single one named Final Service Index (FSI) as shown in Eq. (9). In this equation, some weights are introduced for each of the SI. This is done to cover the different mission requirements that Earth Observation missions can have. Vegetation sensor onboard of SPOT-4 is a great example, because it has been designed explicitly to cover the most of the Earth's surface in the shortest time, considering low space resolution as an acceptable trade-off. One FSI is computed for each of the eight services.

$$FSI = \frac{w_{sr}I_{sr}+w_{tr}I_{tr}+w_{cov}I_{cov}+w_{spctr}I_{spctr}}{w_{sr}+w_{tr}+w_{cov}+w_{spctr}} \tag{9}$$

Once the set of FSIs is obtained, they are finally used to compute the index representing the overall support to the SDGs (named Social Efficiency Index or SEf) as shown in Eq. (10). The integer variable *j* ranges from eon to the number of services that are associated to the goal for which the SEf index is computed.

$$SEf = \frac{\sum FSI_j}{ns} \tag{10}$$

The SDGs Efficiency index also ranges from 0 to 100, where a higher value reflects higher levels of support towards an SDG. For each payload a set of 17 *SEf* is computed, each of them corresponding to the contribution to the specific goal.

3.1 Analysis of a set of VIS-NIR payloads

A set of payloads have been analysed as test cases in the VIS-NIR, TIR and microwave spectral regions.

The VIS-NIR sensors are listed in Table 7. Their specifics are all gathered from ESA [26] and Kramer [18].

Table 7. VIS-NIR analysed payloads. The legend refers to the payloads reported in Fig. 20

Payload	Satellite	Symbol
HRVIR (Nadir)	SPOT-4	▽
HRVIR (Off-Nadir)	SPOT-4	◊
Vegetation	SPOT-4	□
MSI	Sentinel-2	+
OLCI	Sentinel-3	○
SLSTR	Sentinel-3	Δ
UVNS	Sentinel-5	▽
METImage	Sentinel-5	□
AVHRR/3	MetOp	*

The results related to these payloads are shown in Fig. 20, where the SDGs are on x-axis.

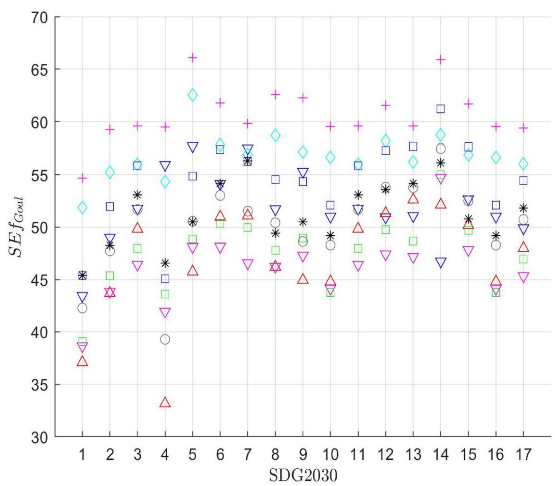

Fig. 20. SDG efficiency index values of VIS-NIR payloads.

The first thing to be noted is that payloads that present good values for all the SI are related to higher SEf values than those sensors that perform well only for specific services. A typical example is given by payloads like Vegetation or AVHRR/3. These have been designed to have a very fast revisit time, accepting a low spacial resolution.

Another interesting aspect is the effect of rotation on narrow swath sensors like HRVIR. The increased swath obtained by the rotation increases HRVIR SEf index compensating the consequent loss of space resolution.

One last comment can be made comparing MSI and HRVIR because MSI is the evolution of HRVIR. It can be clearly seen how the performance of the evolved sensor improved the quality of its data.

3.2 Analysis of a set of TIR payloads

The results of the TIR spectral region focus on the payloads listed in Table 8 and are shown in Fig. 21.

Table 8. TIR analysed payloads. This legend refers to the payloads reported in Fig. 21

Payload	Satellite	Symbol
SLSTR	Sentinel-3	*
METImage	Sentinel-5	+
IASI-NG	Sentinel-5	◊
IASI	MetOp	□
AVHRR/3	MetOp	★
HIRS/4	MetOp	○

In this spectral range the trade-off between refined GSD and fast revisiting time is no longer crucial. The passive payloads operating in TIR region have a very rough GSD due to their operative wavelengths and physical limitations due to their size. Also, revisit times are generally shorter due to the large swaths.

Therefore, the most defining SI becomes the spectral efficiency one. Those sensors that can cover the most part of the considered TIR regions are those who present the best results in terms of SEf.

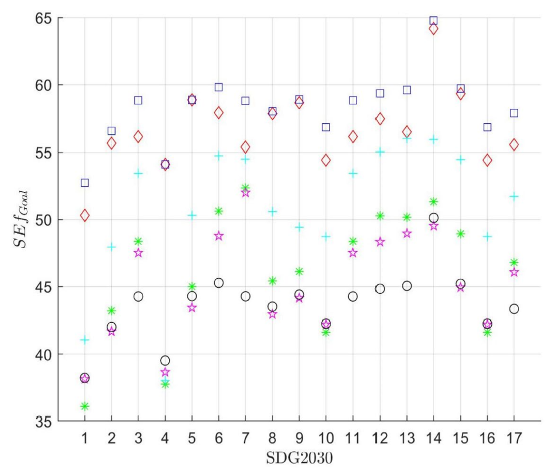

Fig. 21.SDG efficiency index values of TIR payloads.

Another interesting aspect is related to the sensor bandwidth. Those payloads that focus only on TIR region rather than imaging also in VIS-NIR have better SEf results. This is strictly related to the spectral band coverage previously mentioned. The sensors devoting part of their bands to VIS-NIR are usually limited in the coverage of the TIR region.

In this case the difference between obsolete and mature sensors is notable. In fact, even if HIRS/4 is completely devoted to TIR observations, it is the worst sensor analysed in most of the cases.

3.3 Analysis of a set of SAR antennas

As regards the active microwave spectral region use as test cases the sensors reported in Table 9 and the related results are shown in Fig. 22.

Table 9. Analysed SAR antennas. This legend refers to the payloads reported in Fig. 22.

Payload	Satellite	Symbol
C-SAR	Sentinel-1	★
SRAL	Sentinel-3	○
SAR-X	TerraSar-X	□

It can be noted that SAR antennas present generally higher values of SEf indices. This is because they can achieve very good GSD together with relatively large swath.

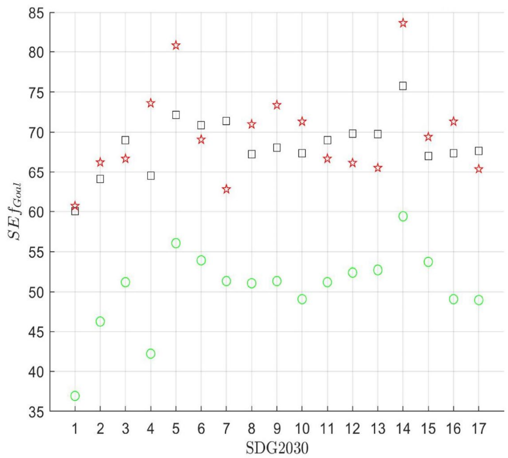

Fig. 22. SDG efficiency index values of SAR antennas

It can be noted that SAR antennas present generally higher values of SEf indices. This is because they can achieve very good GSD together with relatively large swath.

It is interesting to compare two of the best payloads CSAR and SAR-X payloads because of their mixed behaviours as sensors. This occurs because their operative frequency is decided at the design phase and it defines which are the services that will be better achieved. This reflects on quite different FSIs for each service, and as final consequence, on the behaviour of the SEf against the various SDGs. This oscillating result is related to the high specialisation of SAR sensors.

A quick mention about SRAL can be made. It is a small SAR antenna used mainly for altimetry to support the observations of the other payloads onboard of Sentinel-3. Not being the main payload, only a fraction of power is devoted to it and the SEf values show how the performance of this sensor are poor with respect to those payloads who have a fully devoted platform to operate.

4. Quality indices

A set of four complementary indices have been developed, named Quality Indices (QI). These are not related to the SDGs, but they are focused on the quality of the orbital environment where the mission operates according to four aspects that are Earth accessibility, debris danger and severity, orbit crowding, and orbit maintenance effort. These indices do not care about the payload, that have been extensively analysed in the previous SI, but focus on the platform, on its operative orbit and communication capabilities.

4.1 Earth access index

This index analyses how much time with respect to the complete repeat cycle period is in visibility of a ground station belonging to ESTRACK principal and augmented network (ESA [11]).

The position of the spacecraft in the Earth centred rotating frame, r_{sc}, at any time instant is propagated for the whole repeat cycle. The position vectors of the ground stations, r_{gs}, can be evaluated knowing their longitude, Λ_{gs}, and latitude, Φ_{gs}, according to Eq. (11).

$$r_{gs}=\begin{Bmatrix} R_E\cos(\Phi_{gs})\cos(\Lambda_{gs}) \\ R_E\cos(\Phi_{gs})\sin(\Lambda_{gs}) \\ R_E\cos(\Phi_{gs}) \end{Bmatrix} \qquad (11)$$

Using the coverage geometry in Wertz [14], it is possible to compute the aperture angle from the satellite to the Earth, ξ, and its corresponding Earth centre angle, λ, as shown in Fig. 23 following Eq. (12).

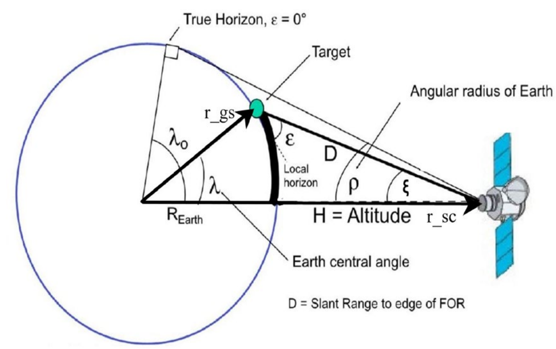

Fig. 23. Earth coverage geometry. Courtesy of Wertz and Larson [14]

$$\begin{gathered} r_\varepsilon = r_{sc} - r_{gs} \\ \xi = acos\left(\frac{r_\varepsilon \cdot r_{sc}}{|r_\varepsilon \cdot r_{sc}|}\right) \\ \lambda = acos\left(\frac{r_{gs} \cdot r_{sc}}{|r_{gs} \cdot r_{sc}|}\right) \\ \varepsilon = 90 - \varepsilon - \lambda \end{gathered} \qquad (12)$$

Once the elevation angle, ε, has been computed it is checked if it is higher than the minimum elevation angle acceptable for communications, typically $\varepsilon_{min} = 5°$ according to Wertz and Larson [14]. When the spacecraft elevation angle is larger than the minimum value, communications are possible. This is not the only condition that must be fulfilled. Indeed, the communication bands of the spacecraft and the ground station must be compatible. If the two conditions are verified, the spacecraft can communicate with the ground station. Following a procedure similar to the one used for the Earth coverage index in Sec. 2.4 and computing the elevation angles from all the compatible ground stations, it is possible to evaluate the time in visibility of at least one ground station that can be used to communicate, named T_{acc}.

The Earth access index is defined as follows in Eq. (13).

$$I_{Ea} = \frac{T_{acc}}{nT_{orbit}} \% \tag{13}$$

4.2 Orbit maintenance index

The orbit maintenance index defines the quality of a mission in terms of orbit maintenance effort. In this paper, the control strategy acts only on the semimajor axis and the inclination. The perturbation affecting the semimajor axis is only the aerodynamic drag while Sun and lunar gravity, solar radiation pressure and Earth J_2 effect cause the change of inclination.

The perturbations to the orbital elements are computed using the modelling proposed by Battin [16].

The control effort is based on Griffin [13] and Fortescue et al. [15] and, both for the semimajor axis and inclination variations.

First, the semimajor axis orbital decay is computed and an acceptable error in position of the groundtrack with respect to the nominal condition E_0 is defined. The strategy proposed by Fortescue et al. [15] and Griffin [13] can be applied, shown in Fig. 24. When the semimajor axis reaches the acceptable minimum value according to E_0, a boosting action raises the orbit up to a maximum altitude that generates a displacement of the groundtrack equal to E_0, but in the opposite direction with respect to the decay.

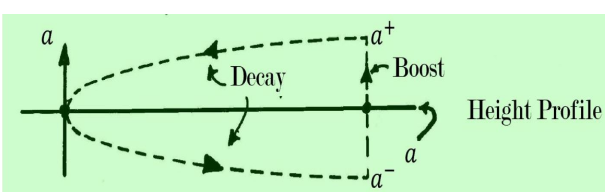

Fig. 24. Semimajor axis control strategy. Courtesy of Griffin [13] and Fortescue et al. [15]

According to the lifetime of the mission, it is possible to compute how many control cycles must be repeated and, consequently, the total ΔV_{drag} of the mission.

A similar strategy is applied to the inclination variation. The acceptable displacement is imposed at a desired latitude because the inclination variation causes a groundtrack drift especially at high latitudes. When the limit drift is reached a small plane change manoeuvre is performed following a very similar strategy to the one used for the semimajor axis. More details can be found in Griffin [13] and Fortescue et al. [15].

The total maintenance velocity change ΔV is computed as the sum of the previous two variations, and the propellant mass, M_{prp}, needed can be derived using Tsiolkovsky equation. In this paper, the propellant LMP-103S is used as reference, described in Anflo [33]. This is a green propellant which is analysed as alternative to hydrazine. The specific impulse associated to the thrusters is $I_{sp} = 235\ s$.

The propellant mass is compared with a reference mass to have a consistent analysis among all the mission in terms of pure maintaining effort rather than dry/wet mass ratio. The baseline value used for this paper is equal to Envisat propellant mass, $M_{ENV} = 320\ kg$. The maintenance index is then computed as follows in Eq. (14).

$$I_{mant} = \frac{M_{prp}}{M_{ENV}} 1000 \tag{14}$$

The maintenance index is characterised to have no upper limit. The lower the value the lower the maintenance effort is. The index is multiplied for a factor 1000 to get a unit scale.

4.3 Debris index

The debris index evaluates the quality of the operative orbits in terms of its exposition to debris and of its debris generation severity. This index is based on the work of Maury et al. [10]. In this work an orbit degradative characterisation factor, *CF,* is computed as the product of a severity characterisation factor, *SF,* and an exposure characterisation factor, *XF*.

The relevant value for this paper is only *CF* that is needed to compute the debris index according to the degradation level of the selected operative orbit. *CF* values for the LEO region are shown in Fig. 25.

It is possible to detect a maximum *CF* level in LEO region, CF_{max}, and use it to compute the debris index, I_{dbr}, as described in Eq. (15).

$$I_{dbr} = \frac{CF_{orbit}}{CF_{max}} \% \tag{15}$$

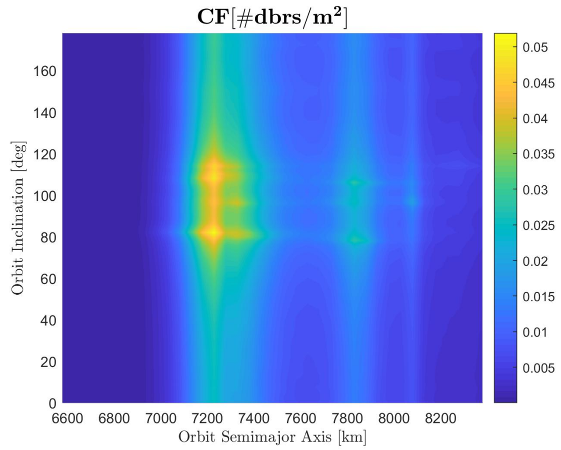

Fig. 25. Orbit degradation characterisation factor. Courtedy of Maury et al. [10]

4.4 Orbit occupation index

This last quality index is designed to assess the quality of a mission basing on the quantity of operative spacecrafts that are occupying the same orbital bin. It can be considered as a complementary of the debris index even if the previous one can be considered as more meaningful.

The quantity of spacecrafts present in LEO region has been obtained by the UCS satellite database [3] and the result is shown in Fig. 26. The same free variables (semimajor axis and inclination) and their intervals used for the debris index have been used to make a direct comparison of these two complementary indices possible.

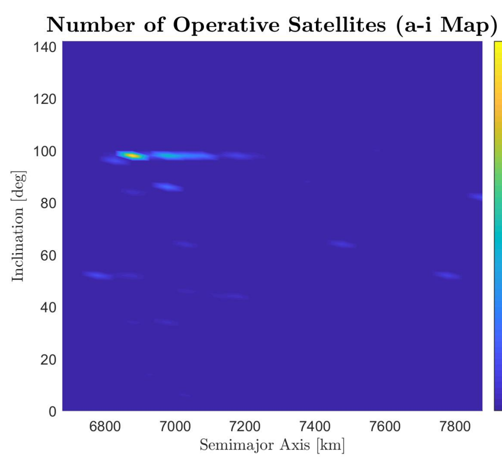

Fig. 26. Number of operative satellites in LEO. Courtesy of UCS [3]

The similarities with the debris index do not stop here. The computation of the orbit occupation index I_{occ} is also very similar to that of the debris index. The baseline quantity is the maximum number of satellites that can be found among the orbital bins in LEO, named $Nsat_{max}$. The occupation index is then computed as shown in Eq. (16).

$$I_{occ} = \frac{Nsat_{orb}}{Nsat_{max}}\% \qquad (16)$$

5. Conclusions

This paper described an innovative method to assess the effectiveness of EO space missions in terms of support to specific services and to the SDGs. The key points of this method are its flexibility, because it can be applied to a generic EO mission in LEO that operates in the VIS-NIR, TIR and microwave spectral regions, and the definition of an index to summarise the quality of the mission according to different services.

As for future planning, the development of new indices to define the quality of a generic space mission can be added. An interesting introduction would be a socio-economic index that compares the social value of the space mission (computable starting from the support to the SDGs) with its production and maintenance cost using a Social Return On Investment (SROI) approach. Another relevant index would be related to the spectral resolution that would be needed to compare the performance of the already well known multispectral and panchromatic sensors with the hyper-spectral ones that are still in development phase.

Moreover, the database of spacecraft sensors can be expanded considering new payloads. Payloads like the passive microwave imagers, LIDARs and active scatterometry sensors can be addressed but they would require a new set of indices because their typical performance is very different from the analysed sensors.

A further study can be done considering constellations which are placed in different orbital planes. This would make the method more general and useful also to analyse, for example, telecommunications missions.

Finally, a more detailed specialisation of the analysed eight services can be done. This would be useful to assess the support of each payload to the single services rather than to the SDGs. The approach chosen in this paper based on eight general services is the best one to assess the relationship with the SDGs.

Acknowledgements

The research leading to these results has received funding from the European Research Council (ERC) under the European Union's Horizon 2020 research and innovation program as part of project COMPASS (Grant agreement No. 679086).

References

[1] ESA, Space debris by the numbers. https://www.esa.int/Our_Activities/Space_Safety/Space_Debris/Space_debris_by_the_numbers., accessed 02.09.2020.
[2] UNOOSA, Online Index of Objects Launched into Outer Space. http://www.unoosa.org/oosa/osoindex/search-ng.jspx., accessed 02.09.2020.
[3] UCS, Operative satellites database. https://www.ucsusa.org/nuclearweapons/spaceweapons/satellitedatabase, accessed 02.09.2020.
[4] Sandau, Rainer, Status and trends of small satellite missions for Earth observation., 2010.
[5] UN, Sustainable Development Goals 2030. https://www.un.org/sustainabledevelopment/sustainabledevelopmentgoals, accessed 02.09.2020.
[6] UNOOSA, Space4SDGs. http://www.unoosa.org/oosa/en/ourwork/space4sdgs/index.html, accessed 02.09.2020.
[7] UNOOSA, European Global Navigation Satellite System and Copernicus: Supporting the Sustainable Development Goals., 2017.
[8] Anderson, Katherine, et al., Earth observation in service of the 2030 Agenda for Sustainable Development., 2017.
[9] Sarelli, Anastasia, et al., A novel automated methodology that estimates the United Nations (UN) Sustainable Development Goal (SDG) 14.1. 1.: index of coastal eutrophication using the Copernicus Marine Environment Monitoring Service (CMEMS), 2018.
[10] Maury, Thibaut, et al., Assessing the impact of space debris on orbital resource in life cycle assessment: A proposed method and case study, 2019.
[11] ESTRACK, ESA's deep space tracking network, https://www.esa.int/Enabling_Support/Operations/ESA_Ground_Stations/Estrack_ground_stations, accessed 02.09.2020.
[12] Curtis, Howard D., Orbital mechanics for engineering students, 2013.
[13] Griffin, Michael Douglas, Space vehicle design, 2004.
[14] James R. Wertz and Wiley J. Larson, Space Mission Analysis and Design, 3rd Ed., 1999.
[15] Fortescue, Peter, Graham Swinerd, and John Stark, eds, Spacecraft systems engineering, 2011.
[16] Battin, Richard H., An Introduction to the Mathematics and Methods of Astrodynamics, revised edition, 1999.
[17] Sissenwine, Norman, Maurice Dubin, and Harry Wexler, The US standard atmosphere, 1962, 1962.
[18] Kramer, Herbert J., Observation of the Earth and its Environment: Survey of Missions and Sensors, 2002.
[19] Moreira, Alberto, et al., A tutorial on synthetic aperture radar., 2013.
[20] Boain, Ronald J., AB-Cs of sun-synchronous orbit mission design., 2004.
[21] Kuenzer, C., Thermal Remote Sensing. https://earth.esa.int/documents/973910/1002056/CK3.pdf/4e5b4e5a-d898-43b8-9e5c-ba7494aa58c8, accessed 03.09.2020.
[22] Baldridge, Alice M., et al., The ASTER spectral library version 2.0., 2009.
[23] Clark, Roger N., et al., USGS digital spectral library splib06a, 2007.
[24] Kokaly, Raymond F., et al., USGS spectral library version 7, 2017.
[25] Meerdink, Susan K., et al., The ECOSTRESS spectral library version 1.0., 2019.
[26] ESA, EO Portal. https://directory.eoportal.org/web/eoportal/satellite-missions, accessed 03.09.2020.
[27] Nowak, D., The impact of microwave penetration depth on the process of heating the moulding sand with sodium silicate, 2017.
[28] Shrestha, Bijay L., Hugh C. Wood, and Shahab Sokhansanj, Modeling of vegetation permittivity at microwave frequencies, 2007.
[29] F. Ulaby, K. McDonald, K. Sarabandi, and M.Dobson, Michigan microwave canopy scatteringmodels (mimics), 1988.
[30] Hallikainen, Martti T., et al., Microwave dielectric behavior of wet soil-part 1: Empirical models and experimental observations, 1985.
[31] Chang, Chieh-Min, Jian-Shiuh Chen, and Tz-Bin Wu, Dielectric modeling of asphalt mixtures and relationship with density, 2011.
[32] Copernicus Programme, COPERNICUS IN SUPPORT OF THE UN SUSTAINABLE DEVELOPMENT GOALS, 2018.
[33] Anflo, Kjell, et al., High performance green propellant for satellite applications, 2009.